Published in final edited form as:
Neuron. 2008 October 9; 60(1): 84–96. doi:10.1016/j.neuron.2008.09.027.

V3 spinal neurons establish a robust and balanced locomotor rhythm during walking

Ying Zhang[1], **Sujatha Narayan**[1], **Eric Geiman**[1], **Guillermo M. Lanuza**[1], **Tomoko Velasquez**[1], **Bayle Shanks**[1], **Turgay Akay**[2,4], **Jason Dyck**[2], **Keir Pearson**[2], **Simon Gosgnach**[1,2], **Chen-Ming Fan**[3], and **Martyn Goulding**[1,*]

[1]Molecular Neurobiology Laboratory, The Salk Institute for Biological Studies, 10010 North Torrey Pines Rd, La Jolla, CA 92037, USA

[2]Department of Physiology, University of Alberta, Medical Science Building, Edmonton, Alberta, T6G 2H7, Canada

[3]Department of Embryology, Carnegie Institution of Washington, 3520 San Martin Drive, Baltimore, MD 21218

Summary

A robust and well-organized rhythm is a key feature of many neuronal networks, including those that regulate essential behaviors such as circadian rhythmogenesis, breathing and locomotion. Here we show that excitatory V3-derived neurons are necessary for a robust and organized locomotor rhythm during walking. When V3-mediated neurotransmission is selectively blocked by the expression of the Tetanus toxin light chain subunit (TeNT), the regularity and robustness of the locomotor rhythm is severely perturbed. A similar degeneration in the locomotor rhythm occurs when the excitability of V3-derived neurons is reduced acutely by ligand-induced activation of the allatostatin receptor. The V3-derived neurons additionally function to balance the locomotor output between both halves of the spinal cord, thereby ensuring a symmetrical pattern of locomotor activity during walking. We propose that the V3 neurons establish a robust and balanced motor rhythm by distributing excitatory drive between both halves of the spinal cord.

Introduction

The simple motor behaviors that underlie locomotion in vertebrates are generated by rhythm generating networks that are embedded in the spinal cord. These networks can function autonomously and are commonly referred to as locomotor central pattern generators (CPGs) (Pearson, 1993; Grillner, 2003; 2006; Kiehn and Kullander, 2004; Goulding and Pfaff, 2005). Lesion and activity studies have mapped the core neuronal elements of the locomotor CPG to the ventral half of the spinal cord (Kjaerulff and Kiehn, 1996; Cowley and Schmidt, 1997), with excitatory and inhibitory CPG interneurons being predominantly localized to lamina VII and lamina VIII. Lamina VII is rich in interneurons whose axons terminate in the ipsilateral ventral horn (Brown, 1981; Saueressig et al., 1999), while lamina VIII contains contralaterally-projecting neurons that cross in the ventral commissure and connect motor networks in both

*To whom correspondence should be addressed. Telephone: (858) 453-4100 x1558; Fax: (858) 450-2172, goulding@salk.edu.
[4]Present Address, Howard Hughes Medical Institute, Center for Neurobiology and Behavior, Columbia University, New York, NY 10012

halves of the spinal cord (Stokke et al., 2002; Moran-Rivard et al., 2001; Pierani et al., 2001; Lanuza et al., 2004; Kiehn, 2006).

Recent developmental studies have identified a number of cardinal classes of interneurons in the embryonic spinal cord that settle in the ventral spinal cord in laminae VII and VIII (Jessell, 2000; Goulding et al., 2002; Goulding and Pfaff, 2005). These interneurons are putative constituents of the locomotor CPG and they are derived from five ventral embryonic interneuron cell types: V0, V1, V2a, V2b and V3 neurons. Recent genetic studies have shed light on the roles that two of these interneuron classes have in shaping motor outputs from the locomotor CPG. V0 neurons, which are predominantly inhibitory commissural interneurons, play an essential role in securing left-right alternation (Lanuza et al., 2004). V1 inhibitory neurons appear to have an evolutionarily conserved role in setting the speed of the locomotor step cycle (Gosgnach et al., 2006). While these studies reveal inhibitory cell types have important roles in shaping the pattern of motor activity during locomotion, inhibitory interneurons are not essential for rhythm generation per se, as rhythmic motor activity can occur in the absence of inhibitory neurotransmission (Cowley and Schmidt, 1995; Bracci et al., 1996; Kremer and Lev-Tov, 1997).

The excitatory cell types that make up the locomotor CPG in walking vertebrates are thought to be derived primarily from two classes of ventral embryonic interneurons: the ipsilaterally-projecting V2a neurons that selectively express Chx10 (Goulding et al., 2002; Kimura et al., 2006; Al-Mosawie et al., 2007; Lundfald et al., 2007), and the Sim1-expressing V3 neurons that arise from p3 progenitors (this study). Other less-well characterized glutamatergic neurons that contribute to motor circuits have also been identified, including excitatory neurons in the cat lumbar cord that receive Group 1 and Group II afferent inputs (Edgley and Jankowska, 1987) and in rodents, the lumbar $Hb9^{+}$ glutamatergic neurons (Hinckley et al., 2005; Wilson et al., 2005) as well as cells that express EphA4 (Kullander et al., 2003; Butt et al., 2005). Aside from evidence indicating that a subset of EphA4-expressing neurons are derived from V2a interneurons (Lundfald et al., 2007), the developmental provenance of these excitatory cell types is not clear.

Studies in the lamprey and frog tadpole have demonstrated a requirement for glutamatergic transmission in rhythm generation (Dale and Roberts, 1985; Roberts et al., 1998; Grillner, 2003). Nonetheless, while it is generally accepted that excitatory neurons have essential roles in locomotor rhythm generation (Grillner, 2003; 2006; Kiehn, 2006; Brownstone and Wilson, 2008), the glutamatergic neurons that are responsible for rhythm generation have not been identified, largely because it has not been possible to identify and selectively manipulate different glutamatergic cell types within the spinal cord. It is thought that the excitatory cells that generate the locomotor rhythm primarily innervate ipsilateral components of the CPG (Grillner, 2003; Kiehn, 2006; McCrea and Rybak, 2008; Brownstone and Wilson, 2008), however, excitatory commissural neurons whose function is not known have also been described in the lamprey and mammalian spinal cord (Buchanan, 1982; Butt and Kiehn, 2003; Kiehn 2006; this study).

In view of the proposed roles for glutamatergic neurons in rhythm generation we set out to comprehensively characterize the V3 population of neurons and determine the functional contribution these cells make to motor outputs from the lumbar spinal cord. We were particularly interested in ascertaining whether neurons derived from the V3 population are required for rhythmogenesis, and/or if they control other aspects of the locomotor rhythm. Here we show that a signature feature of locomotion in animals, namely the production of a robust and balanced locomotor rhythm during walking, is disrupted in mice lacking V3 neuron functionality. We propose that V3-derived neurons ensure a normal walking gait by controlling two important aspects of the locomotor rhythm. First, they are required for the coherent robust

rhythmic bursting of flexor and extensor related motor neurons when fictive walking is induced in the isolated spinal cord. Second, they ensure a proper walking gait by balancing the rhythmic motor outputs that are produced by independent oscillatory locomotor centers in the left and right halves of the spinal cord.

Results

Developmental characterization of V3 spinal neurons

Newborn V3 neurons, which are derived from Nkx2.2/2.9-expressing p3 spinal progenitors, are selectively marked by the expression of the PAS-bHLH transcription factor Sim1 (Briscoe et al., 1999; Goulding et al., 2002). To characterize these cells, sequences encoding Cre recombinase were inserted into the first coding exon of the *Sim1* gene using the strategy previously employed to generate the *Sim1*^{taulacZ} knockin reporter mouse (Figure 1A; Marion et al., 2005). Both the *Sim1*^{Cre}; *R26*$^{floxstop\text{-}lacZ}$ and *Sim1*^{taulacZ} reporter mice exhibited identical patterns of reporter expression (Figure 1B-E, data not shown). At E11.5, the pattern of β-gal reporter expression following *Sim1*^{Cre}-mediated recombination was indistinguishable from endogenous *Sim1* mRNA expression with the *Sim1*-derived β-gal positive cells positioned immediately lateral to Nkx2.2^{+} V3 progenitors (Figure 1C).

At early developmental times, newborn V3 neurons begin to settle ventrally close to the floor plate in a region where locomotor commissural neurons are located (Stokke et al., 2002; Lanuza et al., 2004). Although most of the neurons derived from the V3 population have primary axons that cross the ventral midline (Figure 1E), a small subset of V3 neurons (<15%) possess an ipsilaterally-directed axon, including some cells that have axonal processes in both halves of cord (E.G, M.G, unpublished). The V3 population may thus be unique, in that V3-derived cells located on one side of the cord can project axons to both halves of the spinal cord. Although the V3-derived neurons exhibit a variety of axon morphologies, newborn cells selectively express VGlut2, rather than markers of cholinergic or inhibitory neurons, indicating they are exclusively glutamatergic (Figure 1F-H). This observation is consistent with further analyses showing all of the identified V3-derived presynaptic contacts in the postnatal cord are VGlut2-positive (see Figure 2). These and other findings show that the V3 population generates glutamatergic neurons, most of which project axons to the contralateral half of the cord.

V3 neurons form glutamatergic synaptic contacts with ventral locomotor cell types

To begin assessing whether the V3-derived neurons provide excitation to other locomotor-related neurons in the lumbar spinal cord, mice carrying a single *Sim1*^{Cre} allele were crossed with *R26*$^{floxstop\text{-}GAP43\text{-}GFP}$ reporter mice, this allowing us to visualize the axons of these cells. Examination of *Sim1*^{Cre}; *R26*$^{floxstop\text{-}GAP43\text{-}GFP}$ spinal cords at P0 revealed few, if any, V3 axons within the dorsal horn. In contrast, an extensive network of V3 axonal arbors were present throughout the ventral half of the spinal cord, where premotor interneurons and motor neurons are located (Figure 2A).

We then asked whether V3-derived neurons directly innervate motor neurons that project to muscles that are active during locomotion by injecting the transynaptic viral tracer PRV152 (Smith et al., 2000; Kerman et al., 2003) into various hindlimb muscles. GFP-labeled V3-derived neurons were observed on both the contralateral and ipsilateral sides of the cord 38-40 hrs after making injections into the iliopsoas, a hip flexor and the gastrocnemius, an ankle extensor (Figure 2). This labeling represents monosynaptic connections from V3 neuronal cell types onto motor neurons, as at earlier time points (30-32 hrs post injection), the only cells in the cord that showed PRV152-derived GFP expression were motor neurons in the iliopsoas or gastrocnemius motor pools (Supplemental Figure 1). More than 80% of the V3 neurons transynaptically labeled with PRV152 cords were located on the contralateral side of the spinal

cord and are thus likely to be commissural neurons (Iliopsoas: 88±1.7%, n=656 cells from 4 cords; Gastrocnemius: 84±0.3%, n=197 cells from 3 cords). These findings indicate that most of the excitatory input from V3-derived neurons to motor neurons comes from the contralateral side of the cord.

Confocal microscopy was then used to identify putative synaptic contacts between V3 axon arbors and known locomotor cell types. In sections from P0 *Sim1*^{Cre}; *R26*$^{foxstop\text{-}GAP43\text{-}GFP}$ spinal cords, large numbers of V3-derived glutamatergic contacts were detected on known locomotor neuron cell types, including motor neurons (Figure 2C-F), parvalbumin (PV) expressing Ia inhibitory interneurons (Figure 2G-J), Renshaw cells (Figure 2K-N), Lim3-derived V2 neurons and lamina VIII commissural neurons (data not shown). In optical slices (approx. 1 μm), we found that approximately 22% of the VGlut2$^+$ contacts onto the soma and proximal dendrites of motor neurons (n=14 cells) are derived from V3 neurons, while 24% and 27% of the VGlut2$^+$ contacts onto PV$^+$ Ia inhibitory interneurons (n=9 cells) and Renshaw cells (n=34 cells), respectively, are from V3 axons. These data demonstrate that V3-derived neurons are a major source of excitatory input to motor neurons and other locomotor interneuron cell types.

Cellular properties of V3-derived neurons

Current models for the locomotor CPG predict that a group of excitatory neurons in the ventral cord function as a rhythmogenic center for the locomotor CPG (Kiehn 2006; Brownstone and Wilson, 2008). Since these cells have not been identified, we asked whether the V3-derived neurons in lamina VII/VIII exhibit any of the cellular properties that have been associated with rhythm generation in other CPG circuits (Marder and Bucher, 2001). Whole cell recordings and neurobiotin fills were performed on GFP-labeled V3 cells in the lumbar spinal cord (n=26 cells, Figure 3A and B). Of particular interest were the V3 neurons in lamina VII/VIII that are synaptically coupled to motor neurons. All the V3 cells in laminae VII/VIII (n=14 cells) displayed low cellular capacitances (30-40pF) and high input resistances (range 420-500 MΩ). Furthermore, when injected with a series of prolonged current pulses (30-210pA, 2 secs), these cells typically responded in a linear manner (Figure 3C-F). They exhibited spike frequencies of up to 40Hz with low levels of spike frequency adaptation (Figure 3D and E), their average initial spike frequency being 15.2±4.8 Hz at 120pA. The frequency-current (F-I) response curves for these “ventral” V3 neurons (Figure 3E) were largely linear, with moderate levels of spike frequency adaptation (Figure 3F). These properties suggest that the ventral V3 neurons can generate trains of action potentials that closely follow a range of input currents, properties that would be well suited for neurons with a role in distributing excitation within the locomotor CPG.

Previous studies have shown that neurons participating in rhythm generation often exhibit pronounced sag voltages and post-inhibitory rebound (PIR) in their membrane potential when injected with a hyperpolarizing current (Harris-Warrick and Marder, 1991; Marder and Bucher, 2001). We therefore examined these properties in V3 neurons. The sag voltages for the ventral V3 neurons were small even when the cells were strongly hyperpolarized (15.2+/- 4.9 mV at −120 mV). Moreover few, if any, V3-derived neurons produced an action potential in response to a depolarizing-rebound at hyperpolarizing membrane potentials of less than −100 mV (see example in Figure 3G and H). The potential for V3-derived neurons to function as pacemaker cells was further tested by assessing whether neuromodulators that generate fictive locomotor outputs are capable of inducing rhythmic oscillations in membrane potential, as has been shown for a population of Hb9 interneurons (Wilson et al., 2005). None of the V3 neurons in lamina VII/VIII, when synaptically isolated, showed any underlying oscillatory changes in their membrane potential, either when serotonin (10-20 μM) alone or serotonin (10-20 μM) and dopamine (50-100 μM) were bath applied (data not shown). Furthermore, addition of NMDA

and serotonin at concentrations typically used to induce locomotion (5 and 20 μm, respectively) also failed to induce any change in membrane potential (Figure 3I). Nonetheless, some cells (n=5/18) did show rhythmic changes in membrane potential at high concentrations of NMDA (20 μm). It is unclear whether these cells function as pacemakers, since the NMDA levels that produce these membrane oscillations far exceed those required for fictive locomotion *in vitro*.

Selectively blocking V3-dependent synaptic transmission disrupts the locomotor rhythm

To address the function of the V3 population in shaping motor outputs from the locomotor CPG, we generated the *R26*$^{\text{floxstop-TeNT}}$ strain of mice in which synaptic transmission can be attenuated by the selective expression of the tetanus toxin light chain subunit (TeNT). These mice conditionally express a GFP-TeNT fusion protein following Cre mediated recombination. Initially we tested the *R26*$^{\text{floxstop-TeNT}}$ line with *Nestin*$^{\text{Cre}}$ deletor mice, which efficiently recombines loxP target sites throughout the developing spinal cord (Tronche et al., 1999). *Nestin*$^{\text{Cre}}$-induced widespread recombination, and expression of the GFP-TeNT fusion protein in the P0 spinal cord (Supplemental Figure 2A). This was accompanied by a greater than 100-fold reduction in VAMP2/synaptobrevin levels (Supplemental Figure 2B). The resulting blockade of spinal reflex and locomotor activity (Supplemental Figure 2C and D) is consistent with other studies showing that expression of TeNT effectively blocks neurotransmission in a cell specific manner (Baines et al, 1999; Baines et al., 2001; Yamamoto et al., 2003; Yu et al., 2004). TeNT was then selectively expressed in V3 neurons by crossing mice carrying the *R26*$^{\text{floxstop-TeNT}}$ allele with *Sim1*$^{\text{Cre}}$ mice (Figure 4A,B). In *Sim1*$^{\text{Cre}}$; *R26*$^{\text{floxstopGAP43-GFP}}$; *R26*$^{\text{floxstop-TeNT}}$ mice, we observed the selective loss of VAMP2 in GFP^{+} axon varicosities in the ventral horn indicating VAMP2 is specifically reduced in the axons and axon terminals of V3-derived neurons (Supplemental Figure 3). The widespread loss of VAMP2 from V3 axonal processes argues that TeNT is expressed in the majority of V3-derived neurons.

A comparison of ventral root electroneurogram (ENG) traces from wildtype and *Sim1*$^{\text{Cre}}$; *R26*$^{\text{floxstop-TeNT}}$ cords revealed a marked reduction in the regularity of the locomotor rhythm in many of the *Sim1*$^{\text{Cre}}$; *R26*$^{\text{floxstop-TeNT}}$ cords (Figure 4C-E). This degeneration in the regularity of the locomotor rhythm was observed in both the flexor-related traces that were recorded from the L2 ventral roots and in extensor-related activity measured from the L5 ventral root. The locomotor outputs of *Sim1*$^{\text{Cre}}$; *R26*$^{\text{floxstop-TeNT}}$ cords showed increased variability in the duration of individual motor bursts and in the length of the step cycle period. In many instances this was coupled with a marked asymmetry in the duration of flexor bursts between the left and right halves of the spinal cord (Figure 4C). Further analysis of the motor pattern revealed increased variability in the step cycle period, burst duration and interburst period when V3 neurotransmission was blocked (Figure 4D-F), with the coefficient of variation for both the burst width and the step cycle period of ventral root ENG activity being significantly greater ($p<0.05$) in *Sim1*$^{\text{Cre}}$; *R26*$^{\text{floxstop-TeNT}}$ cords (gray bar; n=10 cords) as compared to control cords (white bar; n=7 cords). When flexor (L2) and extensor (L5) related activity from these recordings were pooled and analyzed, the coefficients of variation for the burst width and step cycle period were 0.115±0.002 and 0.183±0.003 for wildtype cords, and 0.248± 0.006 and 0.277±0.009 for *Sim1*$^{\text{Cre}}$; *R26*$^{\text{floxstop-TeNT}}$ cords (Figure 4G).

A large fraction of the spinal cords from P0 *Sim1*$^{\text{Cre}}$; *R26*$^{\text{floxstop-TeNT}}$ mice also displayed marked differences in their ability to generate any locomotor-like oscillatory activity, either following bath application of NMDA and 5-HT (Figure 5A) or after electrically stimulating sensory afferents (Figure 5B). Whereas high concentrations of 5-HT (≥10 μM) are typically effective in inducing fictive locomotion in wildtype spinal cords (n = 24/24), a significant fraction of the *Sim1*$^{\text{Cre}}$; *R26*$^{\text{floxstop-TeNT}}$ animals (n = 6/20) failed to show any rhythmic motor activity in the presence of 5 μM NMDA and 10 μM 5-HT. At lower concentrations of 5-HT,

the inability of NMDA and 5-HT to induce fictive locomotion in *Sim1*^{Cre}; *R26* $^{flox\text{-}stop\text{-}TeNT}$ cords was even more pronounced with only 7 of 28 cords showing any organized oscillatory activity when perfused with 5 μM NMDA/5 μM 5-HT (Figure 5A). A similar disruption of the locomotor rhythm was observed in P0 *Sim1*^{Cre}*R26*^{floxstopTeNT} cords when stimulation of the sensory afferents was used to induce locomotor-like activity (Figure 5B). Interestingly, in those *Sim1*^{Cre}*R26*^{floxstopTeNT} cords that exhibited some motor bursting, the activity in the contralateral L2 ventral root was largely alternating (Figure 5B). These data demonstrate a significantly reduced ability to produce a stable locomotor rhythm when V3 transmission is blocked.

Sim1^{Cre}; *R26*$^{floxstop\text{-}TeNT}$ spinal cords exhibit asymmetric motor outputs from each half of the cord

A further feature of the altered motor output in *Sim1*^{Cre}; *R26*$^{floxstop\text{-}TeNT}$ spinal cords was the prevalence of marked differences in the duration of flexor-related motor bursts between the left and right L2 ventral roots. In wildtype cords, the locomotor output from both sides of the spinal cord is invariably symmetrical, with the average duration of left and right flexor-related bursts being approximately equivalent. In contrast, cords from *Sim1*^{Cre}; *R26*$^{floxstop\text{-}TeNT}$ animals often exhibited episodes in which the duration of motor bursts in one L2 ventral root were prolonged compared to the other (see Figure 6A and B for an example). In comparing cords from control (n= 8) and *Sim1*^{Cre}; *R26*$^{floxstop\text{-}TeNT}$ (n=9) animals, we observed a significant difference in the coefficients of variation of burst ratio between the left and right halves of the cord (0.132±0.003 and 0.317±0.020, respectively, $p<0.01$). This finding suggests that V3-derived neurons, or a subset thereof, have an important role in matching the motor outputs produced in both halves of the cord during tasks that require a symmetrical motor output, such as walking.

Inhibitory commissural neurons have essential functions in coordinating locomotor activity in both halves of the spinal cord, and are necessary for left-right alternating activity during walking in mice (Lanuza et al., 2004; Kiehn, 2006). The contribution that excitatory commissural neurons make to left-right alternation is less clear, leading us to ask whether the Sim1^{+} V3-derived cells, many of which are excitatory commissural interneurons, might play in coordinating motor activity between both halves of the spinal cord. When circular plot statistics (Zar, 1974) were used to compare the phasing of left-right activity in *Sim1*^{Cre}; *R26*$^{floxstop\text{-}TeNT}$ spinal cords (n = 9) with that of control cords (n=8), a relatively normal pattern of left-right alternating activity was observed (Figure 6C and D). These data argue the V3 population contributes very little to securing left-right alternation during fictive walking.

Acute silencing of V3 neurons results in changes in the locomotor gait

The decreased organization of the locomotor outputs that occurs in the *Sim1*^{Cre}; *R26*$^{floxstop\text{-}TeNT}$ spinal cord led us to ask whether these abnormalities in the motor rhythm might be due to the reconfiguration of the locomotor CPG following the chronic blockade of neurotransmission in the V3 neuron population. To address this issue we asked whether similar changes in the locomotor output are elicited when V3 neuronal activity is reduced using the allatostatin receptor (AlstR) system (Gosgnach et al., 2006; Tan et al., 2006). Spinal cords from *Sim1*^{Cre}; *AlstR192* animals exhibit a normal pattern of motor activity in the absence of the allatostatin ligand (Figure 7A). However, upon addition of allatostatin to these, but not wildtype cords (data not shown), there was a marked degradation of the locomotor output (Figure 7B). The change in the locomotor rhythm was marked by increased variance in the duration of flexor-related bursts between the left and right halves of the spinal cord similar to what is seen when neurotransmission in V3-derived neurons is chronically blocked by TeNT (c.f. Figures 5 and 6). This was coupled with higher variability in the step cycle period, in which the coefficient of variation for the step cycle period was significantly greater ($p<0.05$, n=5 cords)

after applying allatostatin (0.26±0.10) compared to before ligand application (0.14±0.07). These observed defects in rhythmicity, were largely reversed upon washout of the allatostatin peptide (Figure 7C).

A further assessment of the role of V3-derived neurons in walking behaviors was undertaken in awake behaving adult mice. In these experiments, V3-derived neurons in the lumbar cord were "silenced" by directly applying allatostatin to the L2-L4 segments (Akay et al., 2008). Kinematic analysis of walking was analyzed in eight *Sim1*^{Cre}; *AlstR192* animals, five of which showed a profound change in their gait, while three other mice showing either mild or no changes in their gait when allatostatin was applied to the spinal cord. The incomplete penetrance of the phenotype may be due to a number of factors, including differences in ligand accessability, variability in *Sim1*^{Cre}-mediated receptor expression within the V3 population (Supplemental Figure 4), as well as compensatory mechanisms such as sensory feedback compensation. More importantly, a normal gait was always observed when *Sim1*^{Cre}; *AlstR192* cords were treated with saline alone (see Figure 8A), or when allatostatin (upto 1000 μM in saline) was applied to the cords of mice lacking the AlstR (data not shown).

Application of allatostatin to the cord of *Sim1*^{Cre}; *AlstR192* mice (Figure 8B) resulted in a marked increase in the variability of the timing and duration of both the stance and swing phases when these animals walked. In contrast, these same mice displayed a very regular pattern of stepping movements when treated with saline alone (c.f. Figure 8A and B). Many of the *Sim1*^{Cre}; *AlstR192* mice also showed a meandering trajectory in the walkway after allatostatin induced "silencing". This behavior recapitulates the phenotype observed in the *in vitro* spinal cord preparation where there is increased variability in the duration of individual phases of the step cycle during fictive walking. Taken together, these data provide further evidence that the V3 neurons, or a subset thereof, are required for the production of a regular walking rhythm.

Discussion

This study provides a framework for understanding the contribution V3-derived neurons make to the motor circuitry in the spinal cord by characterizing their morphology, neurotransmitter phenotype and cellular properties, and by beginning to define their function during locomotion in mice. Our results demonstrate that V3-derived neurons are necessary for the establishment of a robust, coherent and balanced motor rhythm during walking.

V3 neurons contribute to the coordination of left-right locomotor activity

Motor behaviors such as walking and running in limbed vertebrates require a high degree of bilateral coordination between rhythmic networks in each half of the spinal cord (Grillner, 2003; Grillner, 2006; Kiehn, 2006; Wilson and Brownstone, 2008). There are two essential features of interlimb coordination that underlie these highly symmetrical and repetitive patterns of motor activity. First, the phasing of extensor and flexor motor activity between all four limbs needs to be tightly coordinated. Second, the motor drive to the limb musculature on either side of the animal needs to be balanced with respect to the amplitude and duration of each motor burst. Our findings provide evidence that V3 excitatory commissural connections play a prominent role in the latter, since they are needed for balancing the motor outputs produced in each half of the spinal cord. Our results also provide further support for the idea that inhibitory commissural connections are primarily responsible for coordinating the left-right phasing of the limbs when an animal walks (Cowley and Schmidt, 1995; Lanuza et al., 2004; Kiehn 2006).

We propose that the V3 class of neurons establish a balance between the motor outputs in both halves of the cord by acting on contralateral excitatory and inhibitory locomotor-related neurons in the ventral cord. Many V3-derived neurons are commissural neurons that synapse

directly with hindlimb LMC motor neurons on the opposite side of the spinal cord (Figure 2, E.G and M.G, unpublished). These cells directly excite motor neurons on the contralateral side of the spinal cord, thus coupling the motor drive produced by both halves of the spinal cord. Given the extensive arborization of V3 axons within the ventral horn (Figure 2), the V3 neurons may also modulate locomotor activity in both halves of the cord by providing glutamatergic drive to other excitatory premotor interneurons such as the V2a neurons. In principle, these excitatory pathways would provide a mechanism by which the rhythmic excitatory drive produced in one half of the spinal cord, rather than being localized to that half, would be distributed to locomotor-related neurons in the other half of the cord.

Synaptic inputs from V3-derived neurons onto inhibitory locomotor cell types such as Renshaw cells and putative Ia inhibitory interneurons (see Figure 2) may also contribute to the balancing of motor outputs during fictive locomotion by helping terminate motor bursts. In the adult cat spinal cord Renshaw cells and Ia inhibitory interneurons are active during fictive locomotion where they are active in phase with the motor neurons that they innervate (Pratt and Jordan, 1987). This suggests that both of these inhibitory cell types contribute to the in phase inhibition that shapes each motor burst during fictive stepping rather than the mid-cycle inhibition that controls left-right alternation. The finding the V3 cells make little or no contribution to securing left-right alternation (Figure 6) also fits with our previous observation that V1 neurons, of which Renshaw cells and Ia inhibitory neurons are two subclasses (Alvarez et al., 2005), regulate the speed of stepping movements without affecting left-right alternation (Gosgnach et al., 2006).

Commissural monosynaptic excitatory and disynaptic excitatory-inhibitory commissural inputs to hindlimb motor neurons have been described in rodents (Butt and Kiehn, 2003; Quinlan and Kiehn, 2007), thus raising the possibility that excitatory commissural neurons could contribute to left-right coordination. Nevertheless, commissural connections that depend on glucinergic transmission appear to be the major pathway controlling left-right alternation during walking and swimming (Grillner & Wallén, 1980; Cohen and Harris-Warrick, 1984; Soffe et al, 1984; Jankowska and Noga, 1990; Soffe et al., 2001; Lanuza et al., 2004; Kiehn, 2006). We would therefore like to suggest that two parallel systems may shape left-right locomotor activity in the spinal cord: an “inhibitory” commissural pathway that coordinates the phasing of left and right locomotor networks, and a “V3-excitatory” commissural pathway, which balances the locomotor output across the spinal cord. It is possible that other as yet unidentified excitatory commissural neuron subtypes contribute to left-right alternation, although the $V0_V$ commissural neurons, many of which are excitatory (G.L, unpublished data), appear not to serve this function (Lanuza et al., 2004).

V3- derived neurons and their role in rhythm generation

The question arises as to whether V3 neurons or a subset thereof are core neuronal components of rhythm generating centers in the spinal cord or whether they function as conditionally rhythmic cells. Our findings argue the V3-derived neurons are not absolutely required for oscillatory motor outputs. Only a few of the V3 neurons that we have recorded from exhibit any of the intrinsic cellular properties that are often associated with rhythm-generating pacemaker neurons, namely plateau potentials, conditional bursting properties, strong PIR, and high levels of spike frequency adaptation (Figure 3). Moreover, the connectivity of the ventral V3 neurons differs from what has been proposed for rhythm generating interneurons, namely cells that receive strong sensory innervation from Ia afferents as well as descending serotonergic input from reticulospinal Raphe neurons and are not last order premotor interneurons (McCrea and Rybak, 2008;Brownstone and Wilson, 2008). Nonetheless, a subset of the V3 cells that we recorded from did show underlying oscillations in membrane potential in the presence of high concentrations of NMDA, which is consistent with a role in rhythm

generation. This finding, together with other studies that reveal differences in the intrinsic properties of the more dorsally located V3 neurons, is consistent with the idea that there are multiple V3 neuronal subtypes. The roles that each of these subtypes subserve within the locomotor network and their contribution to rhythm generation remains to be determined.

Notwithstanding the many unresolved details of V3 subtype diversity, connectivity and activity during locomotion, we would like to propose a model in which V3-derived neurons distribute excitatory drive from locomotor rhythm generating centers to other components of the spinal motor network, thereby stabilizing and balancing the locomotor rhythm during behaviors such as walking. V3 neurons in lamina VII and VIII possess high input resistances and respond linearly to current injection over a wide range of firing frequencies (Figure 3), suggesting they may be ideally suited to distributing phasic excitation from rhythm generating cells to other locomotor-related neurons in the ventral cord. The observation that a subset of the V3-derived neurons project axons on both sides of the spinal cord is consistent with such a role and is further evidence that V3 cells couple the locomotor networks in both halves of the spinal cord.

Analyses of other rhythmic systems, including those that produce circadian rhythms demonstrate the important role that neuronal coupling within an oscillatory network plays in the generation of robust rhythmic outputs. This has been shown for both slow photoperiodic oscillators (Aton and Herzog, 2005; Liu et al., 2007) and oscillatory networks that generate fast motor rhythms (Harris-Warrick and Marder, 1991; Orlovsky et al., 1999; Marder and Bucher, 2001; Ramirez et al., 2004; Brownstone and Wilson, 2008). Our data suggests that the coupling of bilaterally segregated oscillatory networks in the spinal cord through V3 commissural connections may confer robustness and fidelity on the locomotor CPG. Interestingly, two coupled oscillatory centers have been identified in the medulla that control respiration (Mellon et al., 2003; Onimaru and Homma, 2003), and it has been hypothesized that coupling between these oscillators increases the robustness of respiratory behaviors. Such coupling between dispersed oscillatory centers may represent a common mechanism for establishing the stable patterns of motor activity that underlie repetitive behaviors such as walking or breathing.

Methods

Generation of *Sim1*^{Cre}; *R26*$^{floxstop\text{-}TeNT}$ mice and ZnG mice

Mice expressing Cre recombinase under the control of *Sim1* regulatory sequences were generated by ES cell gene targeting. Sequences encoding Cre were inserted into the first exon of *Sim1* followed by a PGKneo selection cassette flanked with FRT sites (Figure 1A). Following transmission of the *Sim1*^{Cre} allele through the germline, the FRT–flanked pGKneo cassette was removed. *Sim1*^{Cre} mice were genotyped using primers specific for Cre recombinase (Gosgnach et al., 2006).

R26$^{floxstop\text{-}TeNT}$ mice were generated by replacing the lacZ sequences downstream of a floxed PGKneo-tpA cassette in the *R26* locus (Soriano, 1999) with an open reading frame that encodes a GFP-TeNT fusion protein (Yamamoto et al., 2003).

ZnG reporter mice were generated using the method previously described by Novak et al. (2000). The GFP coding region in the *Z/EG* transgene was modified by the inclusion of a nuclear localization signal (nls) at the N-terminus of the GFP protein. The *ZnG* mouse line was derived from a single founder that showed widespread expression of lacZ.

Animals

The generation and genotyping of mice carrying the *R26*^{lacZ}, *R26*$^{GAP43\text{-}GFP}$, *Sim1*^{taulacZ}, *AlstR192*, *Nestin*^{Cre} and ACTB:Flpe alleles has been described previously (Sapir et al., 2004;

Marion et al., 2005; Lanuza et al., 2004; Gosgnach et al., 2006; Rodriguez et al, 2000). Embryos and postnatal animals obtained from timed matings were genotyped by PCR. *R26*$^{\text{floxstop-TeNT}}$ mice were genotyped using primers specific for the GFP-TeNT allele. Genotyping of *ZnG* mice was performed by tail β-gal staining and PCR using primers specific for lacZ and GFP. All animal experiments were conducted according to the protocols approved by IACUC of the Salk Institute for Biological Studies and NIH guidelines for animal use.

In situ hybridization, β-gal histochemistry, immunohistochemistry and transynaptic tracing

In situ hybridization, β-galactosidase activity detection and immunostainings were performed as described previously (Lanuza et al, 2004; Gosgnach et al, 2006; Sapir et al., 2004).

V3 neuron presynaptic terminals onto identified neurons were mapped in *Sim1*$^{\text{Cre}}$; *R26*$^{\text{floxstop-GAP43-GFP}}$ mice. Images were captured using a Zeiss LSM510 confocal microscope and z-stack reconstructions of the soma and proximal dendrites made from three overlapping 0.5 μm thick optical sections using a 63× oil objective (N.A. 1.25). Points of possible synaptic contact were defined as axon terminations that showed no gap or a slight overlap between the cytoplasmic markers (ChAT, calbindin, and parvalbumin) and GFP immunolabeling. Glutamatergic presynaptic terminals marked by VGluT2 were counted using the same criteria as for GFP-labelled axons. Co-localization of VGluT2 and GFP was a positive indication of a presynaptic terminal and most GFP$^+$ terminals (>95%) contained VGluT2-immunolabeling. Counts of GFP$^+$/VGluT2$^+$ versus VGluT2$^+$ only terminals were used to generate a ratio of V3 IN excitatory synaptic contacts onto motor neurons, Renshaw cells, and Ia inhibitory INs.

Transynaptic tracing from hindlimb motor neurons with PRV152 pseudorabies virus was undertaken using the protocol described in Lanuza et al. (2004). Spinal cords were analysed 38-40 hours after PRV injection, a time previously determined to selectively identify monosynaptic connections to motor neurons (Lanuza et al., 2004).

Electrophysiology

Electrophysiological experiments were performed on spinal cords from early postnatal (P0-P3) mice as described previously (Lanuza et al., 2004; Gosgnach et al., 2006).

Acute Spinal Cord Slice Recordings—For slice recordings, spinal cord slices 250-300 μm thick were cut using a Leica VY1000E vibrating microtome. Following recovery, slices were transferred to a recording chamber mounted on an Olympus BX51W1 microscope and perfused with oxygenated room temperature Ringers solution. GFP$^+$ V3 neurons were visualized using a DAGE-MTI IR-1000 CCD camera and patched visually using a Sutter MPC-325 micromanipulator. Recordings were made in a current clamp mode using a MultiClamp 700B amplifier (Axon Instruments). Patch-clamp recording pipettes of 6-7 MΩ were filled with a solution containing 138 mM K-gluconate, 10 mM KCl, 0.0001 mM $CaCl_2$, 10 mM HEPES, 0.1 mM EGTA, 5 mM Mg-ATP, 0.3 mM GTP-Li, pH 7.4. For each recording 1μg/μl neurobiotin was added to the pipette solution to aid the unambiguous identification of the GFP$^+$ V3 neurons. V3 neurons were isolated synaptically by blocking fast synaptic transmission with TTX (0.1 μM), or a combination of AP-5 (30 μM), CNQX (20 μM), picrotoxin (5 μM) and strychnine (10 μM).

Isolated Whole Cord Recordings—Electroneurogram (ENG) recordings were made in Ringer's solution at room temperature (20°C) by placing bipolar suction electrodes on three of the second and fifth lumbar ventral roots. ENG signals were amplified and bandpass filtered (100Hz-1kHz), digitized and collected using the Axoscope software (Axon Instruments). Rhythmic locomotor activity was induced by adding *N*-methyl-D-aspartic acid (NMDA, 5μM) and 5-hydroxytryptamine (5-HT, 5-20μM,) to the Ringer's solution. The effect of

allatostatin induced V3 silencing was examined by adding the peptide (1μM-5μM) to the perfusion solution (Gosgnach et al., 2006; Tan et al., 2006).

In vivo kinematic analysis

Adult kinematic analyses were performed as described by Akay et al. (2008). Eight adult *Sim1*^{Cre}; *Alstr192* mice (3-6 month old) were anesthetized with isofluorane and given the analgesic buprenorphine (0.1mg/kg). An incision was made in the area of the T11-T13 thoracic vertebrae and the spinal cord exposed via a dorsal laminectomy. The dorsal dura mater was removed and a perfusion bath created using Vaseline. For control experiments, physiological saline was applied to the bath for a period of 20 min. The Vaseline chamber was then removed and the skin above the application site closed using a suture clip. Reflective markers were attached to the iliac crest, hip, knee, ankle, and toe for later kinematic analysis. Isofluorane was then removed and the mouse was placed in a horizontal plexiglass walkway (80cm × 5cm). During locomotor activity, high-speed video recordings were made (Photron FASTCAM) for 30 minutes to monitor leg movements. After recording bouts of locomotion under control conditions, the mouse was anesthetized, the suture clip was removed to expose the spinal cord and allatostatin (500μM to 1mM in saline) was applied to the spinal cord for a period of 20 min. After full recovery from anesthesia, the mouse was then returned to the walkway and locomotor activity was further videotaped for a period of 30 min. High concentrations of allatostatin were used due to the steep concentration gradient that occurs when drugs are applied subdurally (Brumley et al., 2007; Akay et al., 2008). Control animals treated with similar concentrations of allatostatin showed no changes in their locomotor gait. Stick figures of leg movements were constructed using the Peak Motus system.

Data analysis and statistics

We created an open-source package of Octave/Matlab scripts for analyzing the ENG recordings from different ventral roots. This program is available at http://neurodata.sourceforge.org. To characterize the oscillatory behavior of the spinal cord circuits, we calculated power spectrum distributions for rectified and filtered ventral root recordings using the Octave function “pwelch” with a fourier transform window of 100 seconds. Autocorrelation functions were calculated for the same data using the Octave function “xcov” with “coeff” style normalization (“coeff” normalizes the value at lag 0 to 1. To calculate the burst durations, the program was used to determine the length of time between the increase in ventral root discharge rate to half-maximum and the following decrease to half-maximum. Circular statistics (Zar, 1974) were used to determine the coupling strength between ventral roots on the left and right side of the spinal cord.

Student's t tests were performed for each data set. Results were considered statistically significant at $p < 0.05$. All data are expressed as mean ± SD.

Supplementary Material

Refer to Web version on PubMed Central for supplementary material.

Acknowledgments

We thank Jean Rivier for the allatostatin peptide, Phil Soriano for *Rosa26*^{lacZ} mice and Matsuya Yamamoto for the GFP-TeNT expression construct. PRV152 virus stocks were a gift from Lynn Enquist (Princeton). We would like to thank Drs. G. Lemke, C. Stevens, C. Kintner, J. Thomas, O. Britz and F. Stam for their comments. This research was supported by grants from the National Institutes of Health (NS37075 and NS31249 to M.G.) and the Human Frontiers Science Program (HFSP, M.G., K.G.P.). G.M.L. was supported by an HFSP postdoctoral fellowship. E.G. was supported by an NIH NRSA fellowship.

References

Akay T, Fouad K, Pearson KG. New technique for drug application to the spinal cord of walking mice. J Neurosci Meth 2008;171:39–47.

Al-Mosawie A, Wilson JM, Brownstone RM. Heterogeneity of V2-derived interneurons in the adult mouse spinal cord. Eur J Neurosci 2007;26:3003–3015. [PubMed: 18028108]

Alvarez FJ, Jonas PC, Sapir T, Hartley R, Berrocal MC, Geiman EJ, Todd AJ, Goulding M. Postnatal phenotype and localization of spinal cord V1 derived interneurons. J Comp Neurol 2005;493:177–192. [PubMed: 16255029]

Aton SJ, Herzog ED. Come together, right…now synchronization of rhythms in a mammalian circadian clock. Neuron 48:531–534. [PubMed: 16301169]

Baines RA, Uhler JP, Thompson A, Sweeney ST, Bate M. Altered electrical properties in *Drosophila* neurons developing without synaptic transmission. J Neurosci 2001;21:1523–1531. [PubMed: 11222642]

Baines RA, Robinson SG, Fujioka M, Jaynes JB, Bate M. Postsynaptic expression of tetanus toxin light chain blocks synaptogenesis in *Drosophila*. Curr Biol 1999;9:1267–1270. [PubMed: 10556094]

Bracci E, Ballerini L, Nistri A. Localization of rhythmogenic networks responsible for spontaneous bursts induced by strychnine and bicuculline in the rat isolated spinal cord. J Neurosci 1996;16:7063–7076. [PubMed: 8824342]

Briscoe J, Sussel L, Serup P, Hartigan-O'Connor D, Jessell TM, Rubenstein JL, Ericson J. Homeobox gene Nkx2.2 and specification of neuronal identity by graded Sonic hedgehog signalling. Nature 1999;398:622–627. [PubMed: 10217145]

Brown, AG. Organization of the spinal cord. NewYork: springer-Verlag; 1981.

Brownstone RM, Wilson JM. Strategies for delineating spinal locomotor rhythm-generating networks and the possible role of Hb9 interneurones in rhythmogenesis. Brain Res Rev 2008;57:64–76. [PubMed: 17905441]

Brumley MR, Hentall ID, Pinzon A, Kadam BH, Blythe A, Sanchez FJ, Taberner AM, Noga BR. Serotonin concentrations in the lumbosacral spinal cord of the adult rat following microinjection or dorsal surface application. J Neurophysiol 2007;98:1440–1450. [PubMed: 17634342]

Buchanan JT. Identification of neurons with contralateral, caudal axons in the lamprey spinal cord: Synaptic interactions and morphology. J Neurophysiol 1982;47:961–975. [PubMed: 6177842]

Butt SJ, Kiehn O. Functional identification of interneurons responsible for left-right coordination of hindlimbs in mammals. Neuron 2003;38:953–963. [PubMed: 12818180]

Butt SJ, Lundfald L, Kiehn O. EphA4 defines a class of excitatory locomotor-related interneurons. Proc Natl Acad Sci USA 2005;102:14098–14103. [PubMed: 16172411]

Cohen AH, Harris-Warrick RM. Strychnine eliminates alternating motor output during fictive locomotion in the lamprey. Brain Res 1984;293:164–167. [PubMed: 6704713]

Cowley KC, Schmidt BJ. Effects of inhibitory amino acid antagonists on reciprocal inhibitory interactions during rhythmic motor activity in the in vitro neonatal rat spinal cord. J Neurophysiol 1995;74:1109–1117. [PubMed: 7500136]

Cowley KC, Schmidt BJ. Regional distribution of the locomotor pattern-generating network in the neonatal rat spinal cord. J Neurophysiol 1997;77:247–259. [PubMed: 9120567]

Dale N, Roberts A. Dual-component amino-acid-mediated synaptic potentials: excitatory drive for swimming in *Xenopus* embryos. J Physiol 1985;363:35–59. [PubMed: 2862278]

Edgley SA, Jankowska E. An interneuronal relay for group I and group II muscle afferents in the midlumbar segments of the cat spinal cord. J Physiol 1987;389:647–674. [PubMed: 3681739]

Gosgnach S, Lanuza GM, Butt SJ, Saueressig H, Zhang Y, velasquez T, Riethmacher D, Callaway EM, Kiehn O, Goulding M. V1 spinal neurons regulate the speed of vertebrate locomotor outputs. Nature 2006;440:215–219. [PubMed: 16525473]

Goulding M, Lanuza G, Sapir T, Narayan S. The formation of sensorimotor circuits. Curr Opin Neurobiol 2002;12:508–515. [PubMed: 12367629]

Goulding M, Pfaff SL. Development of circuits that generate simple rhythmic behaviors in vertebrates. Curr Opin Neurobiol 2005;15:14–20. [PubMed: 15721739]

Grillner S. The motor infrastructure: from ion channels to neuronal networks. Nat Rev Neurosci 2003;4:573–586. [PubMed: 12838332]

Grillner S. Biological pattern generation: the cellular and computational logic of networks in motion. Neuron 2006;52:751–766. [PubMed: 17145498]

Grillner S, Wallén P. Does the central pattern generation for locomotion in lamprey depend on glycine inhibition? Acta Physiol Scand 1980;110:103–105. [PubMed: 7468266]

Harris-Warrick RM, Marder E. Modulation of neural networks for behavior. Ann Rev Neurosci 1991;14:39–57. [PubMed: 2031576]

Hinckley C, Hartley R, Wu L, Todd A, Ziskin-Conhaim L. Locomotor-like rhythms in a genetically distinct cluster of interneurons in the mammalian spinal cord. J Neurophysiol 2005;93:1439–1449. [PubMed: 15496486]

Jankowska E, Noga BR. Contralaterally projecting lamina VIII interneurons in the middle lumbar segments of the cat. Brain Res 1990;535:327–330. [PubMed: 2073610]

Jessell TM. Neuronal specification in the spinal cord: inductive signals and transcriptional codes. Nat Rev Genet 2000;1:20–29. [PubMed: 11262869]

Kerman IA, Enquist LW, Watson SJ, Yates BJ. Brainstem substrates of sympatho-motor circuitry identified using trans-synaptic tracing with pseudorabies virus recombinants. J Neurosci 2003;23:4657–4666. [PubMed: 12805305]

Kjaerulff O, Kiehn O. Distribution of networks generating and coordinating locomotor activity in the neonatal rat spinal cord in vitro: a lesion study. J Neurosci 1996;16:5777–5794. [PubMed: 8795632]

Kiehn O. Locomotor circuits in the mammalian spinal cord. Annu Rev Neurosci 2006;29:279–306. [PubMed: 16776587]

Kiehn O, Kullander K. Central pattern generators deciphered by molecular genetics. Neuron 2004;41:317–321. [PubMed: 14766172]

Kimura Y, Okamura Y, Higashijima S. Alx, a zebrafish homolog of Chx10, marks ipsilateral descending excitatory interneurons that participate in the regulation of spinal locomotor circuits. J Neurosci 2006;26:5684–5697. [PubMed: 16723525]

Kremer E, Lev-Tov A. Localization of the spinal network associated with the generation of hindlimb locomotion in the neonatal rat and organization of its transverse coupling system. J Neurophysiol 1997;77:1155–1170. [PubMed: 9084588]

Kullander K, Butt SJ, Lebret JM, Lundfald L, Restrepo CE, Rydstrom A, Klein R, Kiehn O. Role of EphA4 and EphrinB3 in local neuronal circuits that control walking. Science 2003;299:1889–1892. [PubMed: 12649481]

Lanuza GM, Gosgnach S, Pierani A, Jessell TM, Goulding M. Genetic identification of spinal interneurons that coordinate left-right locomotor activity necessary for walking movements. Neuron 2004;42:375–386. [PubMed: 15134635]

Liu AC, Welsh DK, Ko CH, Tran HG, Zhang EE, Priest AA, Buhr ED, Singer O, Meeker K, Verma IM, Doyle FJ, Takahashi JS, Kay SA. Intercellular coupling confers robustness against mutations in the SCN circadian clock network. Cell 2007;129:605–616. [PubMed: 17482552]

Lundfald L, Restrepo CE, Butt SY, Peng CY, Droho S, Endo T, Zeilhofer HU, Sharma K, Kiehn O. Phenotype of V2-derived interneurons and their relationship to the axon guidance molecule EphA4 in the developing spinal cord. Eur J Neurosci 2007;26:2989–3002. [PubMed: 18028107]

McCrea DA, Rybak IA. Organization of mammalian locomotor rhythm and pattern generation. Brain Res Rev 2008;57:134–146. [PubMed: 17936363]

Marder E, Bucher D. Central pattern generators and the control of rhythmic movements. Curr Biol 2001;11:R986–R996. [PubMed: 11728329]

Marion JF, Yang C, Caqueret A, Boucher F, Michaud JL. Sim1 and Sim2 are required for the correct targeting of mammillary body axons. Development 2005;132:5527–5537. [PubMed: 16291793]

Mellon NM, Janczewski WA, Bocchiarro CM, Feldman JL. Opoid-induced quantal slowing reveals dual networks for respiratory rhythm generation. Neuron 2003;37:821–826. [PubMed: 12628172]

Moran-Rivard L, Kagawa T, Saueressig H, Gross MK, Burrill J, Goulding M. *Evx1* is a postmitotic determinant of V0 interneuron identity in the spinal cord. Neuron 2001;29:385–399. [PubMed: 11239430]

Novak A, Guo C, Yang W, Nagy A, Lobe C. Z/EG, a double reporter mouse line that expresses enhanced green fluorescent protein upon Cre-mediated excision. Genesis 2000;28:147–155. [PubMed: 11105057]

Onimaru H, Homma I. A novel functional neuron group for rhythm generation in the ventral medulla. J Neurosci 2003;23:1478–1486. [PubMed: 12598636]

Orlovsky, GN.; Deliagina, TG.; Grillner, S. Neural control of locomotion. Oxford University Press; Oxford, UK: 1999.

Pearson KG. Common principles of motor control in vertebrates and invertebrates. Ann Rev Neurosci 1993;16:265–297. [PubMed: 8460894]

Pierani A, Moran-Rivard L, Sunshine MJ, Littman DR, Goulding M, Jessell TM. Control of interneuron fate in the developing spinal cord by the progenitor homeodomain protein Dbx1. Neuron 2001;29:367–384. [PubMed: 11239429]

Pratt CA, Jordan LM. Ia inhibitory interneurons and Renshaw cells as contributors to the spinal mechanisms of fictive locomotion. J Neurophysiol 1987;57:56–71. [PubMed: 3559681]

Quinlan KA, Kiehn O. Segmental, synaptic actions of commissural interneurons in the mouse spinal cord. J Neurosci 2007;27:6521–6530. [PubMed: 17567813]

Ramirez JM, Tryba AK, Pena F. Pacemaker neurons and neuronal networks: an integrative overview. Curr Opin Neurobiol 2004;14:665–674. [PubMed: 15582367]

Roberts A, Soffe SR, Wolf ES, Yoshida M, Zhao FY. Central circuits controlling locomotion in young frog tadpoles. Ann NY Acad Sci 1998;860:19–34. [PubMed: 9928299]

Rodríguez CI, Buchholz F, Galloway J, Sequerra R, Kasper J, Ayala R, Stewart AF, Dymecki SM. High-efficiency deleter mice show that FLPe is an alternative to Cre-loxP. Nat Genet 2000;25:139–140. [PubMed: 10835623]

Saueressig H, Burrill J, Goulding M. Engrailed-1 and netrin-1 regulate axon pathfinding by association interneurons that project to motor neurons. Development 1999;126:4201–4212. [PubMed: 10477289]

Smith BN, Banfield BW, Smeraski CA, Wilcox CL, Dudek FE, Enquist LW, Pickard GE. Pseudorabies virus expressing enhanced green fluorescent protein: A tool for in vitro electrophysiological analysis of transsynaptically labeled neurons in identified central nervous system circuits. Proc Natl Acad Sci USA 2000;97:9264–9269. [PubMed: 10922076]

Sapir T, Geiman EJ, Wang Z, Velasquez T, Mitsui S, Yoshihara Y, Frank E, Alvarez FJ, Goulding M. *Pax6* and *Engrailed 1* regulate two distinct aspects of Renshaw cell development. J Neurosci 2004;24:1255–1264. [PubMed: 14762144]

Soffe SR, Clarke JDW, Roberts A. Activity of commissural interneurons in the spinal cord of *Xenopus* embryos. J Neurophysiol 1984;51:1257–1267. [PubMed: 6737030]

Soffe SR, Zhao FY, Roberts A. Functional projection distances of spinal interneurons mediating reciprocal inhibition during swimming in *Xenopus* tadpoles. Eur J Neurosci 2001;13:617–627. [PubMed: 11168570]

Soriano P. Generalized *lacZ* expression with the ROSA26 Cre reporter strain. Nat Genet 1999;21:70–71. [PubMed: 9916792]

Stokke MF, Nissen UV, Glover JC, Kiehn O. Projection patterns of commissural interneurons in the lumbar spinal cord of the neonatal rat. J Comp Neurol 2002;446:349–359. [PubMed: 11954034]

Tan EM, Yamaguchi Y, Horwitz GD, Gosgnach S, Lein ES, Goulding M, Albright TD, Callaway EM. Selective and quickly reversible inactivation of mammalian neurons in vivo using the *Drosophila* allatostatin receptor. Neuron 2006;51:157–170. [PubMed: 16846851]

Tronche F, Kellendonk C, Kretz O, Gass P, Anlag K, Orban PC, Bock R, Klein R, Schütz G. Disruption of the glucocorticoid receptor gene in the nervous system results in reduced anxiety. Nat Genet 1999;23:99–103. [PubMed: 10471508]

Wilson JM, Hartley R, Maxwell DJ, Todd AJ, Lieberam I, Kaltschmidt JA, Yoshida Y, Jessell TM, Brownstone RM. Conditional rhythmicity of ventral spinal interneurons defined by expression of the Hb9 homeodomain protein. J Neurosci 2005;25:5710–5719. [PubMed: 15958737]

Yamamoto M, Wada N, Kitabatake Y, Watanabe D, Anzai M, Yokoyama M, Teranishi Y, Nakanishi S. Reversable suppression of glutamatergic neurotransmission of cerebellar granule cells in vivo by

genetically regulated expression of tetanus neurotoxin light chain. J Neurosci 2003;23:6759–6767. [PubMed: 12890769]

Yu CR, Power J, Barnea G, O'Donnell S, Brown HE, Osborne J, Axel R, Gogos JA. Spontaneous neural activity is required for the establishment and maintainance of the olfactory sensory map. Neuron 2004;42:553–566. [PubMed: 15157418]

Zar, JH. Biostatistical Analysis. Englewood-Cliffs, NJ: Prentice Hall; 1974.

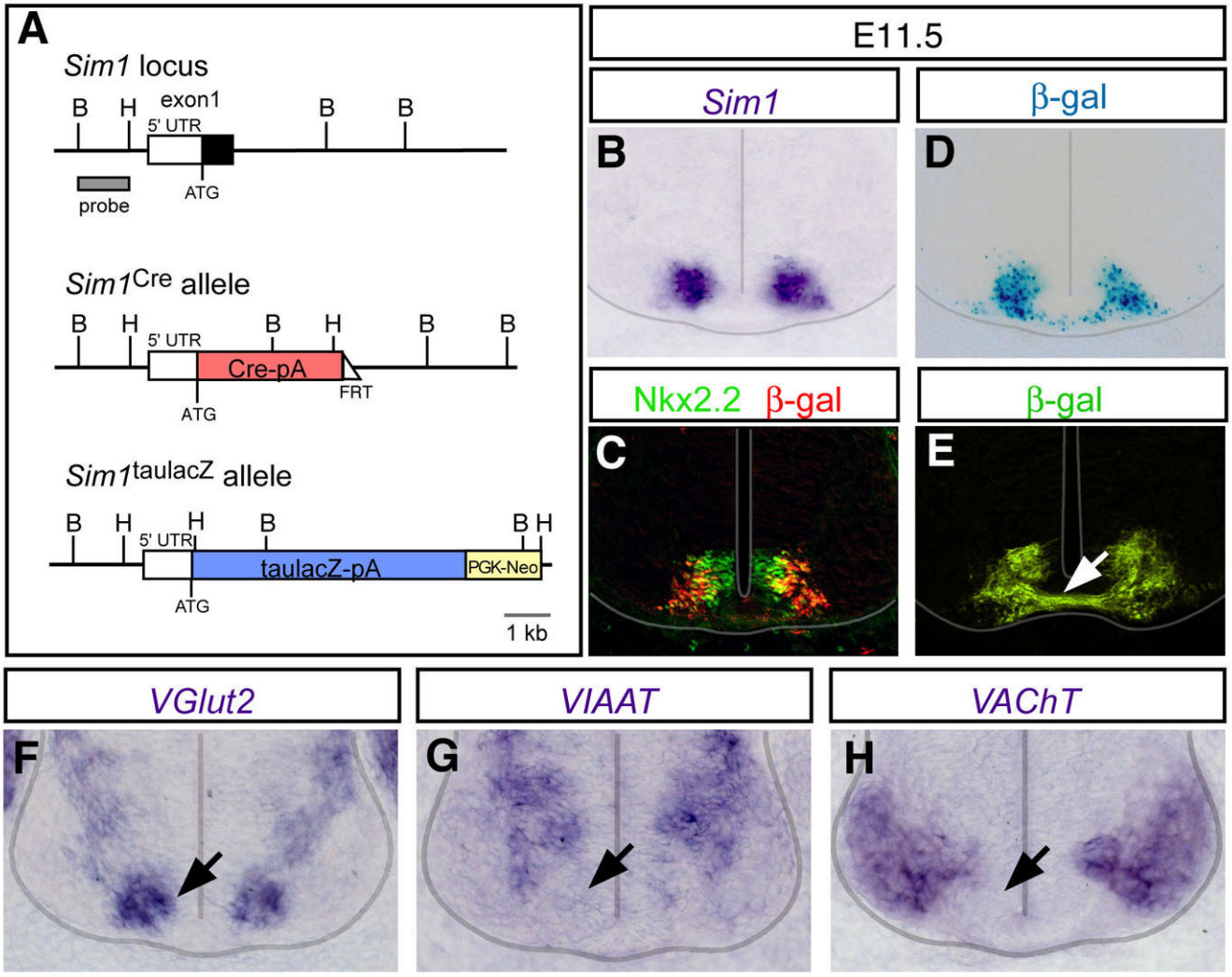

Figure 1. Generation and characterization of *Sim1*^{Cre} and *Sim1*^{taulacZ} mice

(A) Schematic diagrams of wild type *Sim1* locus and the targeted *Sim1* alleles. Gene cassettes encoding *Cre* recombinase and *taulacZ* were inserted into the first exon of the *Sim1* gene to generate the *Sim1*^{Cre} and *Sim1*^{taulacZ} alleles, respectively. The FRT-flanked neomycin cassette in the *Sim1*^{Cre} allele was removed by crossing *Sim1*^{Cre} founder mice with an ACTB:Flpe transgenic line.

(B-D) Analysis of *Sim1*^{Cre} mediated recombination. *Sim1*^{Cre} mice were crossed with *Rosa26*$^{floxstop\text{-}lacZ}$ (*R26*^{lacZ}) reporter mice (Soriano, 1999). (B) The distribution of *Sim1* transcripts at E11.5. (C) Immunohistochemistry showing that β-gal^{+} cells (red) arise from Nkx2.2-expressing p3 progenitors (green). (D) β-galactosidase activity in V3 neurons (D) is comparable to *Sim1* expression (B).

(E) Analysis of *Sim1*^{taulacz} E11.5 spinal cord showing V3 neurons project axons across the ventral midline (arrow).

(F-H) In situ hybridization of markers for glutamatergic (*VGlut2*), inhibitory (*VIAAT*) and cholinergic (*VAChT*) neurons at E11.5 showing *VGlut2* is selectively expressed in the V3 domain (arrow).

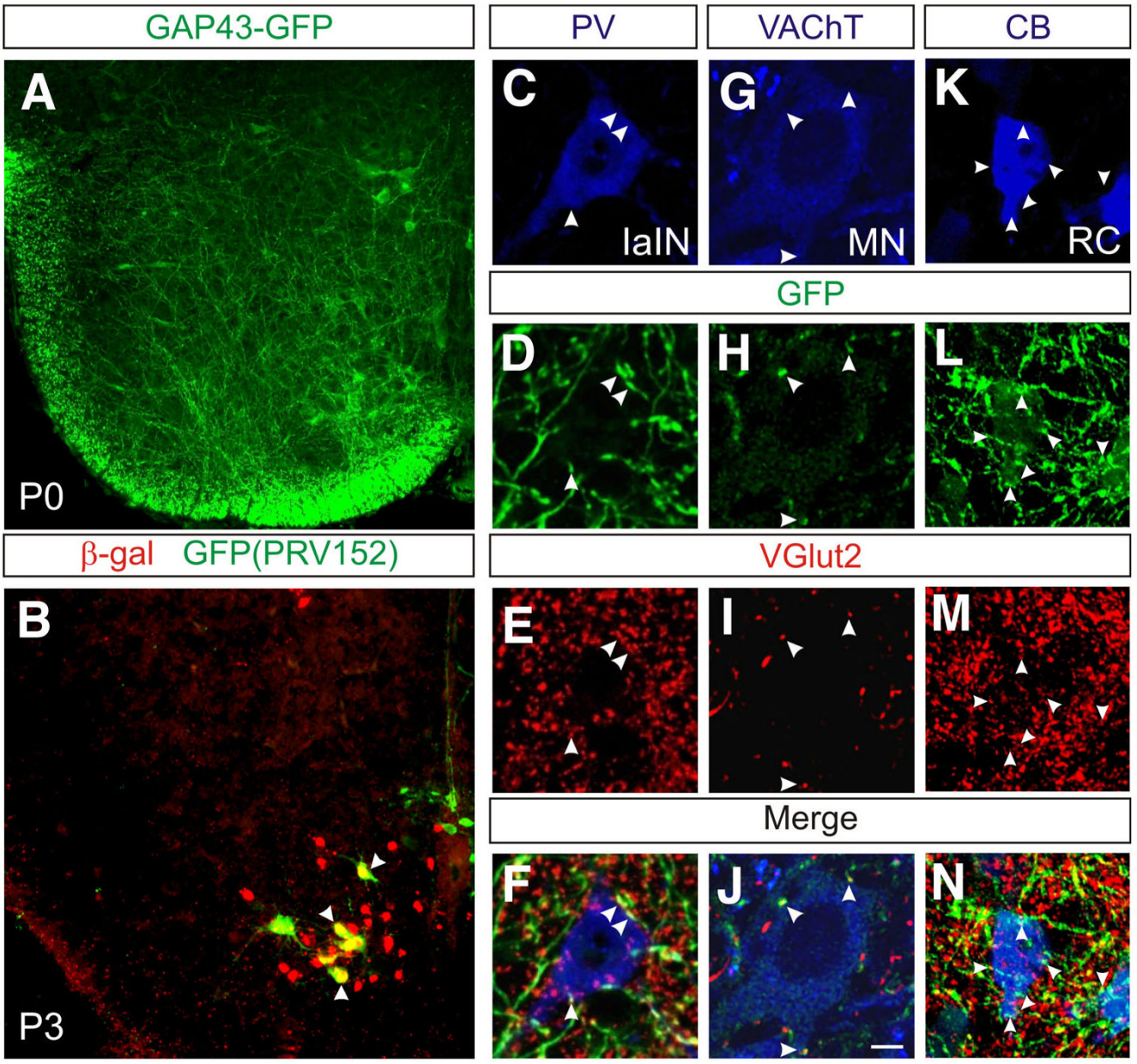

Figure 2. V3-derived neurons are glutamatergic neurons that make synaptic contacts on motor neurons and locomotor-related interneurons

(A) Transverse upper lumbar spinal cord section in *Sim1*^{Cre}; *R26*$^{floxstop\text{-}GAP43\text{-}GFP}$ mice at P0 reveals the presence of GFP-labeled V3-derived axons throughout the ventral spinal cord. **(B)** Transynaptic labeling of spinal cord interneurons in *Sim1*^{Cre}; *R26*$^{floxstop\text{-}lacZ}$ mice by PRV152. Injections of PRV152 into hindlimb muscles shows that V3-derived neurons synapse with contralateral motor neurons. Note the co-localization of β-gal (red) and GFP in V3 commissural neurons that are transynaptically labeled with PRV152 (arrowheads). **(C-N)** In *Sim1*^{Cre}; *R26*$^{floxstop\text{-}GAP43\text{-}GFP}$ mice, V3 axons (GFP, green) make glutamatergic contacts (red, arrowheads) onto Ia inhibitory interneurons (IaIN, C-F) that express parvalbumin (PV, blue), onto VAChT-immunolabeled (blue) motor neurons (G-J) and onto calbindin^{+}

Renshaw cells (K-N). Images C-F and K-N are from P18 spinal cords whereas images G-J are from a P0 spinal cord.

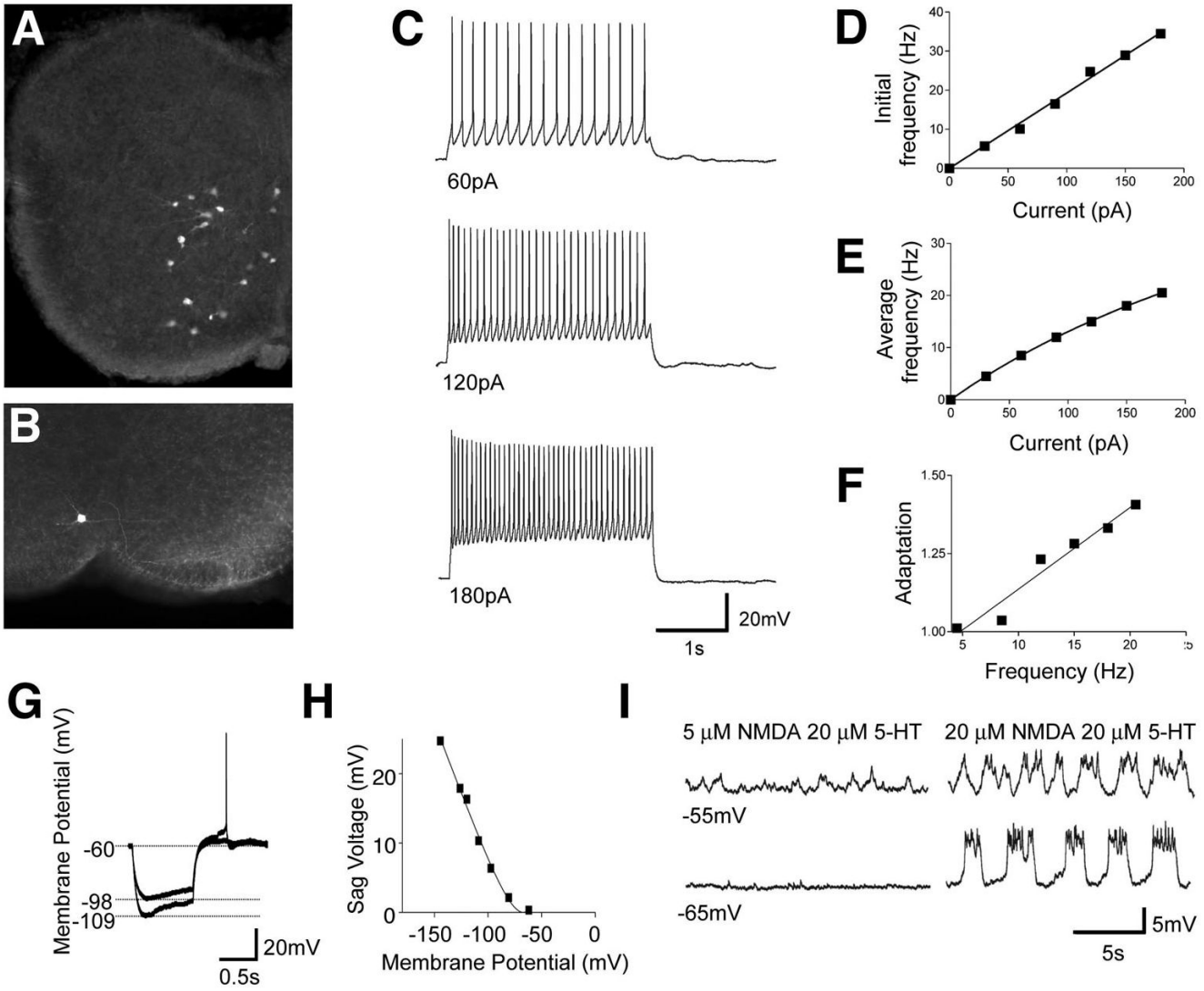

Figure 3. Cellular properties of V3-derived neurons in lamina VIII

(A) Vibratome slice from P0 *Sim1*^{Cre}; ZnG spinal cord showing V3-derived neurons expressing GFP.

(B) An example of a whole cell patch-clamp recorded V3 neuron labeled with neurobiotin.

(C and D) Representative response of a ventral V3-derived neuron to a series of 2s depolarizing currents (C). A linear relationship was found in the initial spike frequency as a function of the increasing input currents (D).

(E) The relationship of the average spike frequency as a function of the input current was fitted by a non-linear regression function (Y=a*x/(1+x/b)).

(F) A moderate but linear increase in the spike frequency adaptation was found along the increasing spike frequency (n==14 cells). The level of spike adaptation was determined by the average of the last three spike frequencies divided by the average of the first-three spike frequencies for varying 2 second current steps. Current steps of 20–210 pA were applied to each cell.

(G-H) Small to moderate sag voltages and post rebound potentials were produced by a series of 1 s hyperpolarizing currents in lamina VII/VIII V3 neurons. The amplitude of the sag voltage was strongly voltage dependent (H).

(I) Some V3-derived neurons display slow oscillations in membrane potential in the presence of 20 μM NMDA/20 μM 5-HT but not 5 μM NMDA/20 μM 5-HT.

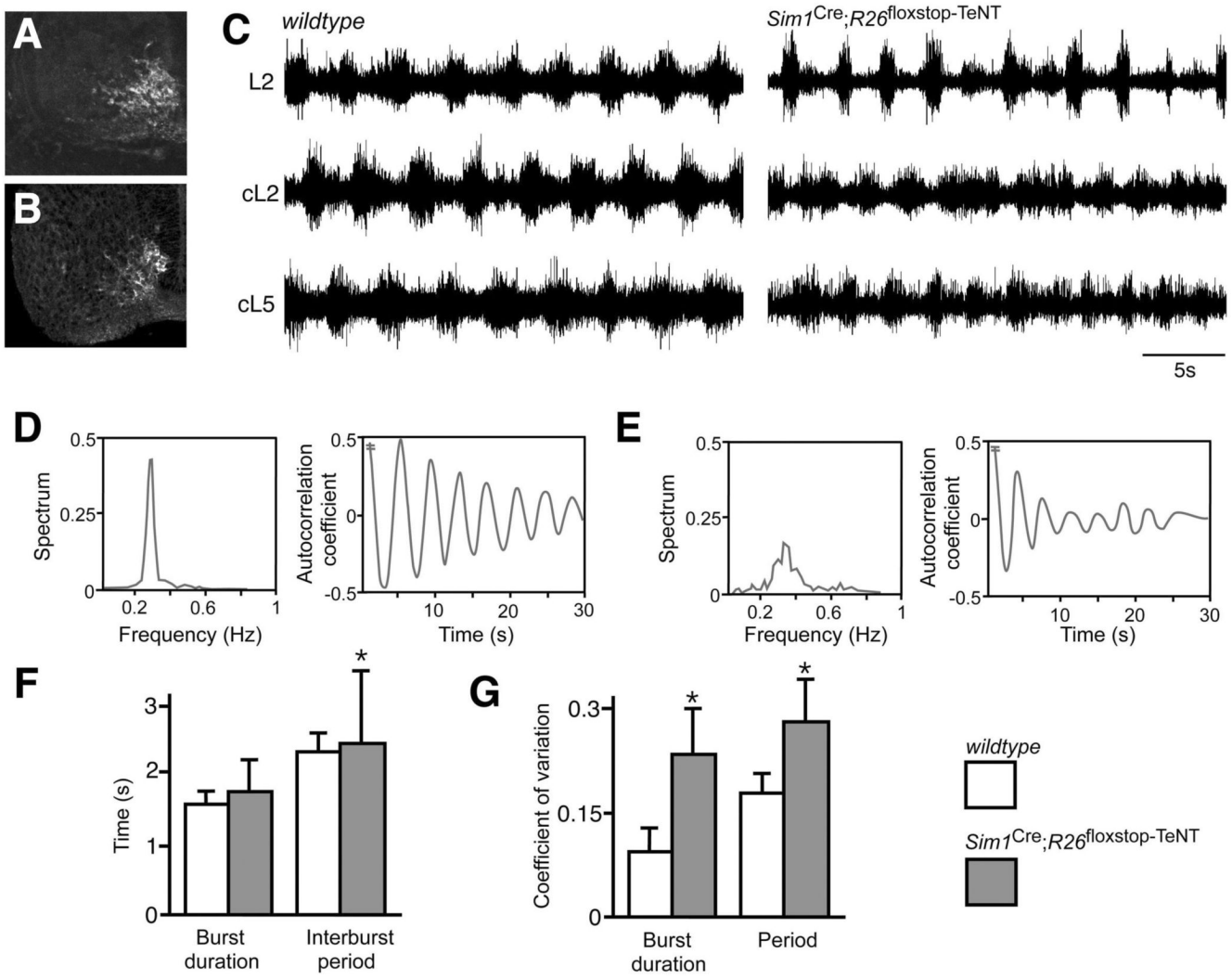

Figure 4. Suppression of the synaptic transmission of V3-derived neurons disrupts the locomotor rhythm

(A-B) Comparison of β-gal staining in *Sim1*^{taulacZ} E12.5 spinal cord (A) and GFP expression in *Sim1*^{Cre}; *R26*$^{floxstop\text{-}TeNT}$ embryos (B) showing selective expression of the GFP-tetanus toxin light chain subunit fusion protein (GFP-TeNT) in V3-derived neurons.

(C) Extracellular recordings from L2, contralateral L2 (cL2) and the cL5 ventral roots of wildtype (left) and *Sim1*^{Cre}; *R26*$^{floxstop\text{-}TeNT}$ (right) P0 animals.

(D and E) Recordings from the L2 ventral root in wildtype control cords exhibit a narrow peak for the power spectrum distribution of oscillatory frequency (D, left). Spinal cords from *Sim1*^{Cre};*R26*$^{floxstop\text{-}TeNT}$ animals exhibit a broad frequency band (E, left). Autocorrelation coefficient analysis on L2 ventral root recordings shows the oscillatory outputs from *Sim1*^{Cre}; *R26*$^{floxstop\text{-}TeNT}$ spinal cords show a strong reduction in coherency (E, right) compared to wildtype animals (D, right). The average time constant decay for the autocorrelation plot was -0.067±0.001s and -0.117±0.004s for wildtype and *Sim1*^{Cre}; *R26*$^{floxstop\text{-}TeNT}$ animals, respectively ($p<0.05$). Note that the autocorrelation is equal to 1 at time 0 (not shown).

(F and G) *Sim1*^{Cre}; *R26*$^{floxstop\text{-}TeNT}$ cords show increased variability in burst duration, interburst period, and step cycle period compared to cords isolated from control animals. Lines indicate standard deviation. The coefficient of variation (CV) of the burst width (left) and the

oscillation period (right) of ventral root ENGs (E,F) were significantly greater ($p<0.05$) in *Sim1*^{Cre}; *R26*$^{floxstop\text{-}TeNT}$ animals (gray) than in wildtypes (white). Asterisk indicates significant difference from the control.

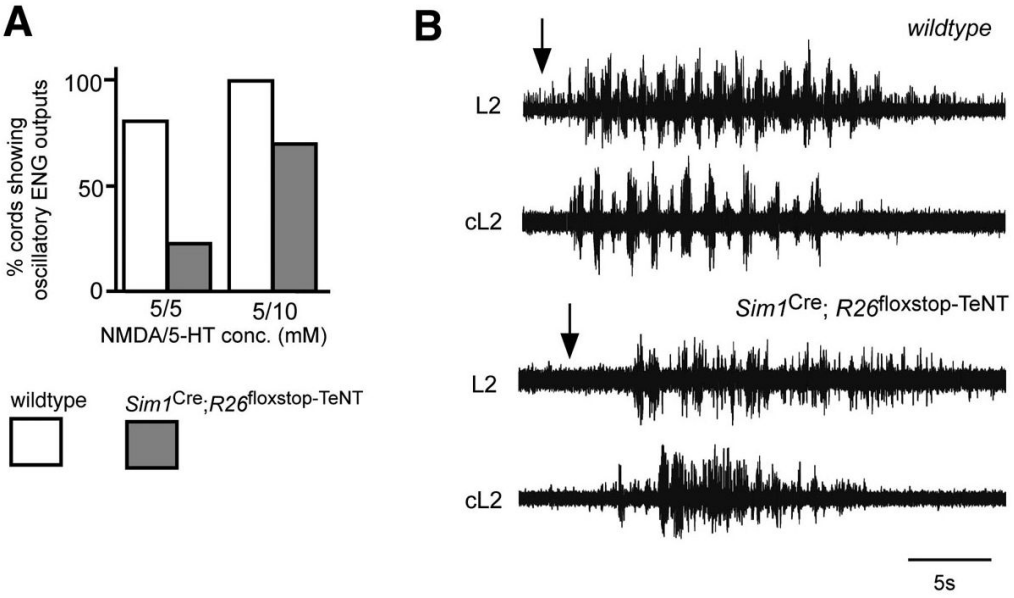

Figure 5. Attenuation of neurotransmission in V3-derived neurons impairs fictive locomotion

(A) *Sim1*^{Cre}; *R26*$^{floxstop\text{-}TeNT}$ spinal cords (gray bars) show impaired production of locomotor-like oscillations following the application of NMDA and 5-HT (5 μM/5 μM (left) and 5 μM/ 10 μM (right), respectively) when compared to wildtype animals (white bars).

(B) Recordings of flexor–related L2 motor activity reveals a decrease in locomotor–like oscillatory outputs following electrical stimulation of L3 sensory roots in the *Sim1*^{Cre}; *R26*$^{floxstop\text{-}TeNT}$ cord (lower traces) compared to the wildtype cord (upper traces). Most *Sim1*^{Cre}; *R26*$^{floxstop\text{-}TeNT}$ cords displayed a highly degraded pattern of flexor motor activity.

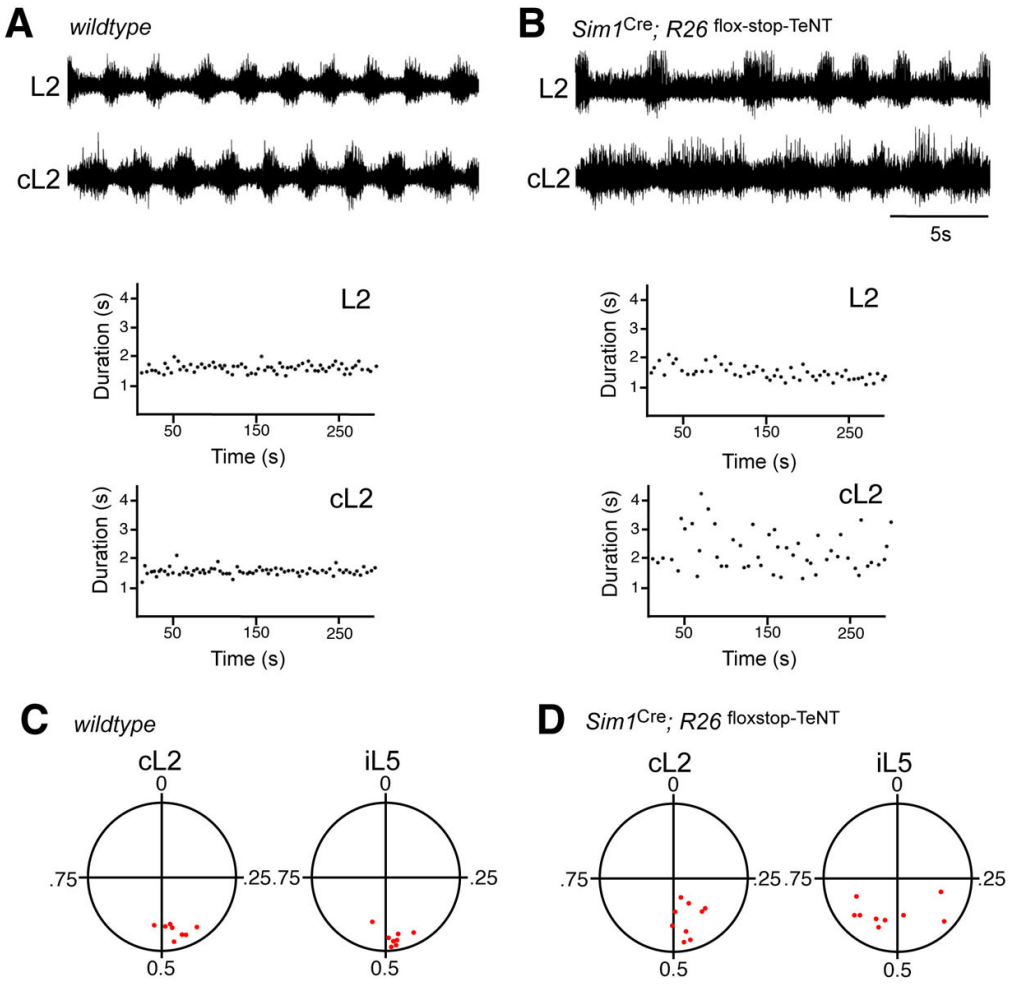

Figure 6. *Sim1*^{Cre}; *R26*$^{floxstop\text{-}TeNT}$ animals display asymmetrical patterns of left-right activity during drug-induced locomotion

(A,B) Example of ENG recordings made from left and right L2 ventral roots over a prolonged period (>10 min) of stable locomotor activity induced by NMDA (5 μM) and 5-HT (10 μM). Control wildtype cords (C) typically exhibit a stable pattern of locomotor activity marked by low variance in the cycle to cycle burst duration for each L2 ventral root. *Sim1*^{Cre}; *R26*$^{floxstop\text{-}TeNT}$ spinal cords show an asymmetrical pattern of flexor-related motor activity between both halves of the spinal cord, together with the high cycle to cycle variability in the burst duration period (D). While the duration of flexor-related burst activity in the left and right halves of spinal cords are closely matched, the cL2 bursts in this *Sim1*^{Cre}; *R26*$^{floxstop\text{-}TeNT}$ cord were prolonged compared to the other L2 ventral root. The lower panels show the burst duration for the flexor-related recording shown above over a 5 minute period. Note the increased variability and asymmetry in the step cycle period in the *Sim1*^{Cre}; *R26*$^{floxstop\text{-}TeNT}$ cord (L2, 2.70±0.67 secs, range 1.62-4.30 secs; cL2 1.72±0.27 secs, range 1.37-2.67 secs) compared to the control cord (L2, 1.59±0.10 secs, range 1.24-1.92 secs; cL2, 1.53±0.14 secs, range 1.27-1.90 secs).

(C, D) Circular plots (Zar, 1974) showing the phase coupling between right L2 (cL2) and left L5 (iL5) with respect to left L2 ventral roots over a 5 minute period of stable locomotor-like activity. Each point represents the calculated vector point for a single spinal cord. Points located near 0.5 represent alternation, while those near 1 represent coactivation. Note left-right alternation (cL2) is normal in the majority of the *Sim1*^{Cre}; *R26*$^{floxstop\text{-}TeNT}$ cords.

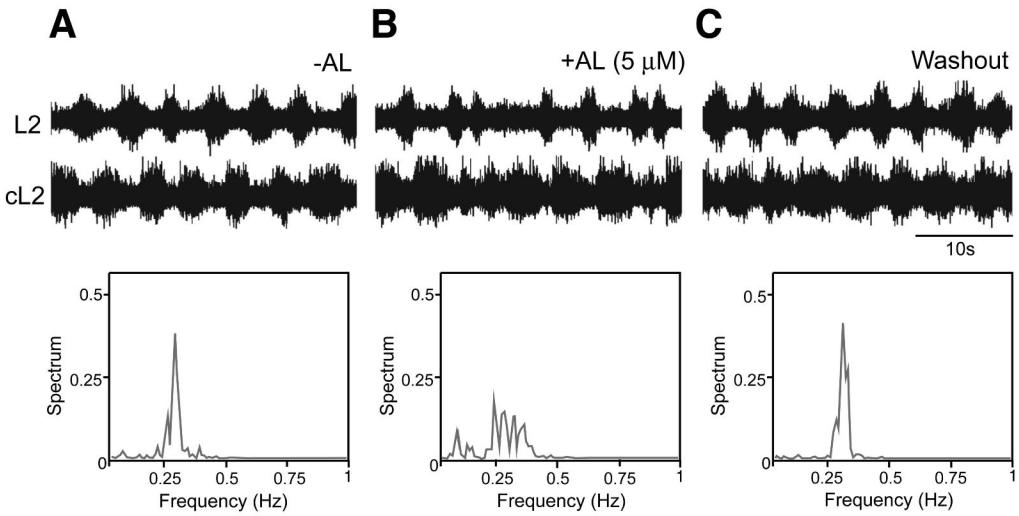

Figure 7. Acute suppression of the V3 neuronal activity disturbed the locomotion activity

(A-C) Extracellular ventral root recordings from left and right L2 ventral roots of a P1 *Sim1*^{Cre}; *AlstR192* mouse before (A), during (B) and after (C, washout) application of 2μM allatostatin peptide. Activation of the allatostatin receptor in V3-derived neurons leads to a decrease in the rhythmicity of locomotor-like outputs during NMDA and 5-HT induced bouts of fictive locomotion. Power spectrum distribution of L2 ventral root oscillatory frequency before, during and after the application of the synthetic ligand (lower panels) show increased variance in the step cycle period when allatostatin is present.

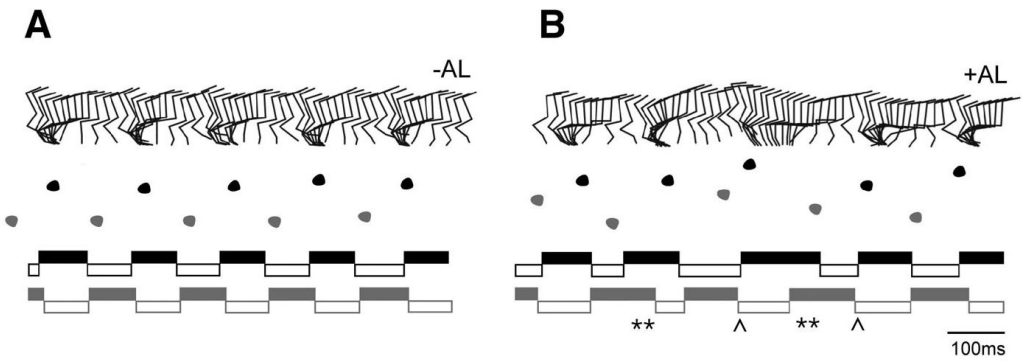

Figure 8. Allatostatin-induced attenuation of V3 neuronal activity in adult *Sim1*^{Cre}; *AlstR192* mice

Kinematic analysis of *Sim1*^{Cre}; *AlstR192* mice before and after application of allatostatin ligand to the lumbar spinal cord. ACSF alone (left) and 1mM allatostatin in ACSF (right) were applied to the exposed spinal cord (L2-L4 segments) of a *Sim1*^{Cre}; *AlstR192* mouse.

Upper panels: Stick diagrams illustrating the stance and swing movements of the left hindlimb. Allatostatin application causes a disordered gait as illustrated by the increased variability in timing and phasing of stepping movements. Middle panels: Foot placement analysis during the same walking sequence, which shows increased variability in the positioning of the hind paw following application of allatostatin. Note the meandering trajectory following application of allatostatin. Lower panels: Stance phase (solid bars) and swing phase (empty bars) for the left (L) and right (R) hindlimbs during the same bout of locomotion. Application of allatostatin causes a marked disruption in the duration and timing of the stance and swing phases. Periods of substantial overlap between the stance (extensor) phase of the left and right hindlimbs are indicated by a double asterisk. Skipping movements involving overlapping swing (flexor) phases for the left and right hindlimbs are indicated by a chevron.